Long-range angular correlations on the near and away side in p–Pb collisions at $\sqrt{s_{NN}} = 5.02$ TeV ☆

ALICE Collaboration

A B S T R A C T

Angular correlations between charged trigger and associated particles are measured by the ALICE detector in p–Pb collisions at a nucleon–nucleon centre-of-mass energy of 5.02 TeV for transverse momentum ranges within $0.5 < p_{T,assoc} < p_{T,trig} < 4$ GeV/c. The correlations are measured over two units of pseudorapidity and full azimuthal angle in different intervals of event multiplicity, and expressed as associated yield per trigger particle. Two long-range ridge-like structures, one on the near side and one on the away side, are observed when the per-trigger yield obtained in low-multiplicity events is subtracted from the one in high-multiplicity events. The excess on the near-side is qualitatively similar to that recently reported by the CMS Collaboration, while the excess on the away-side is reported for the first time. The two-ridge structure projected onto azimuthal angle is quantified with the second and third Fourier coefficients as well as by near-side and away-side yields and widths. The yields on the near side and on the away side are equal within the uncertainties for all studied event multiplicity and p_T bins, and the widths show no significant evolution with event multiplicity or p_T. These findings suggest that the near-side ridge is accompanied by an essentially identical away-side ridge.

© 2013 CERN. Published by Elsevier B.V. All rights reserved.

1. Introduction

Two-particle correlations are a powerful tool to explore the mechanism of particle production in collisions of hadrons and nuclei at high energy. Such studies involve measuring the distributions of relative angles $\Delta\varphi$ and $\Delta\eta$ between pairs of particles: a "trigger" particle in a certain transverse momentum $p_{T,trig}$ interval and an "associated" particle in a $p_{T,assoc}$ interval, where $\Delta\varphi$ and $\Delta\eta$ are the differences in azimuthal angle φ and pseudorapidity η between the two particles.

In proton–proton (pp) collisions, the correlation at ($\Delta\varphi \approx 0$, $\Delta\eta \approx 0$) for $p_{T,trig} > 2$ GeV/c is dominated by the "near-side" jet peak, where trigger and associated particles originate from a fragmenting parton, and at $\Delta\varphi \approx \pi$ by the recoil or "away-side" jet [1]. The away-side structure is elongated along $\Delta\eta$ due to the longitudinal momentum distribution of partons in the colliding protons. In nucleus–nucleus collisions, the jet-related correlations are modified and additional structures emerge, which persist over a long range in $\Delta\eta$ on the near side and on the away side [2–14]. The shape of these distributions when decomposed into a Fourier series defined by v_n coefficients [15] is found to be dominated by contributions from terms with $n = 2$ and $n = 3$ [6,7,9–14]. The v_n coefficients are sensitive to the geometry of the initial state of the colliding nuclei [16,17] and can be related to the transport

properties of the strongly-interacting de-confined matter via hydrodynamic models [18–20].

Recently, measurements in pp collisions at a centre-of-mass energy $\sqrt{s} = 7$ TeV [21] and in proton–lead (p–Pb) collisions at a nucleon–nucleon centre-of-mass energy $\sqrt{s_{NN}} = 5.02$ TeV [22] have revealed long-range ($2 < |\Delta\eta| < 4$) near-side ($\Delta\varphi \approx 0$) correlations in events with significantly higher-than-average particle multiplicity. Various mechanisms have been proposed to explain the origin of these ridge-like correlations in high-multiplicity pp and p–Pb events. These mechanisms include colour connections forming along the longitudinal direction [23–26], jet-medium [27] and multi-parton induced [28,29] interactions, and collective effects arising in the high-density system possibly formed in these collisions [30–35].

Results from two-particle correlations in $\sqrt{s_{NN}} = 0.2$ TeV d–Au collisions [36,37] show a strong suppression of the away-side yield at forward rapidity in central collisions. This modification has been interpreted in the framework of "Colour Glass Condensate" models [38] as a saturation effect caused by nonlinear gluon interactions in the high-density regime at small longitudinal parton momentum fraction x. Similar effects may arise at midrapidity in p–Pb collisions at $\sqrt{s_{NN}} = 5.02$ TeV, where the parton distributions are probed down to $x < 10^{-3}$, which is comparable to the relevant range of x at forward rapidity ($y \sim 3$) at $\sqrt{s_{NN}} = 0.2$ TeV.

This Letter presents results extracted from two-particle correlation measurements in p–Pb collisions at $\sqrt{s_{NN}} = 5.02$ TeV, recorded with the ALICE detector [39] at the Large Hadron Collider (LHC). The correlations are measured over two units of

pseudorapidity and full azimuthal angle as a function of charged-particle multiplicity, and expressed as associated yield per trigger particle. Sections 2 and 3 describe the experimental setup, and the event and track selection, respectively. Details on the definition of the correlation and the per-trigger-particle associated yield are given in Section 4. The results of the analysis are discussed in Section 5 and a summary is given in Section 6.

2. Experimental setup

Collisions of proton and lead beams were provided by the LHC during a short pilot run performed in September 2012. The beam energies were 4 TeV for the proton beam and 1.58 TeV per nucleon for the lead beam, resulting in collisions at $\sqrt{s_{NN}} = 5.02$ TeV. The nucleon–nucleon centre-of-mass system moved with respect to the ALICE laboratory system with a rapidity of -0.465, i.e., in the direction of the proton beam. The pseudorapidity in the laboratory system is denoted with η throughout this Letter. Results from pp collisions at $\sqrt{s} = 2.76$ and 7 TeV are shown in comparison to the p–Pb results.

A detailed description of the ALICE detector can be found in Ref. [39]. The main subsystems used in the present analysis are the Inner Tracking System (ITS) and the Time Projection Chamber (TPC), which are operated inside a solenoidal magnetic field of 0.5 T. The ITS consists of six layers of silicon detectors: from the innermost to the outermost, two layers of Silicon Pixel Detector (SPD) with an acceptance of $|\eta| < 1.4$, two layers of Silicon Drift Detector (SDD) with $|\eta| < 0.9$ and two layers of Silicon Strip Detector with $|\eta| < 0.97$. The TPC provides an acceptance of $|\eta| < 0.9$ for tracks which reach the outer radius of the TPC and up to $|\eta| < 1.5$ for tracks with reduced track length. The VZERO detector, two arrays of 32 scintillator tiles each, covering the full azimuth within $2.8 < \eta < 5.1$ (VZERO-A) and $-3.7 < \eta < -1.7$ (VZERO-C), was used for triggering, event selection and event characterization, namely the definition of event classes corresponding to different particle-multiplicity ranges. In p–Pb collisions, the trigger required a signal in either VZERO-A or VZERO-C. In addition, two neutron Zero Degree Calorimeters (ZDCs) located at $+112.5$ m (ZNA) and -112.5 m (ZNC) from the interaction point are used in the event selection. The energy deposited in the ZNA, which for the beam setup of the pilot run originates from neutrons of the Pb nucleus, served as an alternative approach in defining the event-multiplicity classes. In pp collisions, the trigger required a signal in either SPD, VZERO-A or VZERO-C [40].

3. Event and track selection

The present analysis of the p–Pb data is based on the event selection described in Ref. [41]. The events are selected by requiring a signal in both VZERO-A and VZERO-C. From the data collected, 1.7×10^6 events pass the event selection criteria and are used for this analysis. For the analysis of the pp collisions, the event selection described in Ref. [40] has been used, yielding 31×10^6 and 85×10^6 events at $\sqrt{s} = 2.76$ and 7 TeV, respectively.

The primary-vertex position is determined with tracks reconstructed in the ITS and TPC as described in Ref. [42]. The vertex reconstruction algorithm is fully efficient for events with at least one reconstructed primary track within $|\eta| < 1.4$ [43]. An event is accepted if the coordinate of the reconstructed vertex along the beam direction (z_{vtx}) is within ± 10 cm from the detector centre. The analysis uses tracks reconstructed in the ITS and TPC with $0.5 < p_T < 4$ GeV/c and in a fiducial region $|\eta| < 1.2$. As a first step in the track selection, cuts on the number of space points and the quality of the track fit in the TPC are applied. Tracks are further required to have a distance of closest approach to the

Table 1

Definition of the event classes as fractions of the analyzed event sample and their corresponding $\langle dN_{ch}/d\eta \rangle$ within $|\eta| < 0.5$ and the mean numbers of charged particles within $|\eta| < 1.2$ and $p_T > 0.5$ GeV/c. The given uncertainties are systematic as the statistical uncertainties are negligible.

Event class	V0M range (a.u.)	$\langle dN_{ch}/d\eta \rangle|_{|\eta|<0.5}$ $p_T > 0$ GeV/c	$\langle N_{trk} \rangle|_{|\eta|<1.2}$ $p_T > 0.5$ GeV/c
60–100%	<138	6.6 ± 0.2	6.4 ± 0.2
40–60%	138–216	16.2 ± 0.4	16.9 ± 0.6
20–40%	216–318	23.7 ± 0.5	26.1 ± 0.9
0–20%	>318	34.9 ± 0.5	42.5 ± 1.5

reconstructed vertex smaller than 2.4 cm and 3.2 cm in the transverse and the longitudinal direction, respectively. In order to avoid an azimuthally-dependent tracking efficiency due to inactive SPD modules, two classes of tracks are combined [44]. The first class consists of tracks, which have at least one hit in the SPD. The tracks from the second class do not have any SPD associated hit, but the position of the reconstructed primary vertex is used in the fit of the tracks. In the study of systematic uncertainties an alternative track selection [45] is used, where a tighter p_T-dependent cut on the distance of closest approach to the reconstructed vertex is applied. Further, the selection for the tracks in the second class is changed to tracks, which have a hit in the first layer of the SDD. This modified selection has a less uniform azimuthal acceptance, but includes a smaller number of secondary particles from interactions in the detector material or weak decays.

The efficiency and purity of the primary charged-particle selection are estimated from a Monte Carlo (MC) simulation using the DPMJET event generator [46] (for p–Pb) and the PYTHIA 6.4 event generator [47] with the tune Perugia-0 [48] (for pp) with particle transport through the detector using GEANT3 [49]. In p–Pb collisions, the combined efficiency and acceptance for the track reconstruction in $|\eta| < 0.9$ is about 82% at $p_T = 0.5–1$ GeV/c, and decreases to about 79% at $p_T = 4$ GeV/c. It reduces to about 50% at $|\eta| \approx 1.2$ and is independent of the event multiplicity. The remaining contamination from secondary particles due to interactions in the detector material or weak decays decreases from about 2% to 1% in the p_T range from 0.5 to 4 GeV/c. The contribution from fake tracks is negligible. These fractions are similar in the analysis of pp collisions.

In order to study the multiplicity dependence of the two-particle correlations the selected event sample is divided into four event classes. These classes are defined fractions of the analyzed event sample, based on cuts on the total charge deposited in the VZERO detector (V0M), and denoted "60–100%", "40–60%", "20–40%", "0–20%" from the lowest to the highest multiplicity in the following. Table 1 shows the event-class definitions and the corresponding mean charged-particle multiplicity densities ($\langle dN_{ch}/d\eta \rangle$) within $|\eta| < 0.5$. These are obtained using the method presented in Ref. [41], and are corrected for acceptance and tracking efficiency as well as contamination by secondary particles. Also shown are the mean numbers of primary charged particles with $p_T > 0.5$ GeV/c within the pseudorapidity range $|\eta| < 1.2$. These are measured by applying the track selection described above and are corrected for the detector acceptance, track-reconstruction efficiency and contamination.

4. Analysis

For a given event class, the two-particle correlation between pairs of trigger and associated charged particles is measured as a function of the azimuthal difference $\Delta\varphi$ (defined within $-\pi/2$ and $3\pi/2$) and pseudorapidity difference $\Delta\eta$. The correlation is expressed in terms of the associated yield per trigger particle for
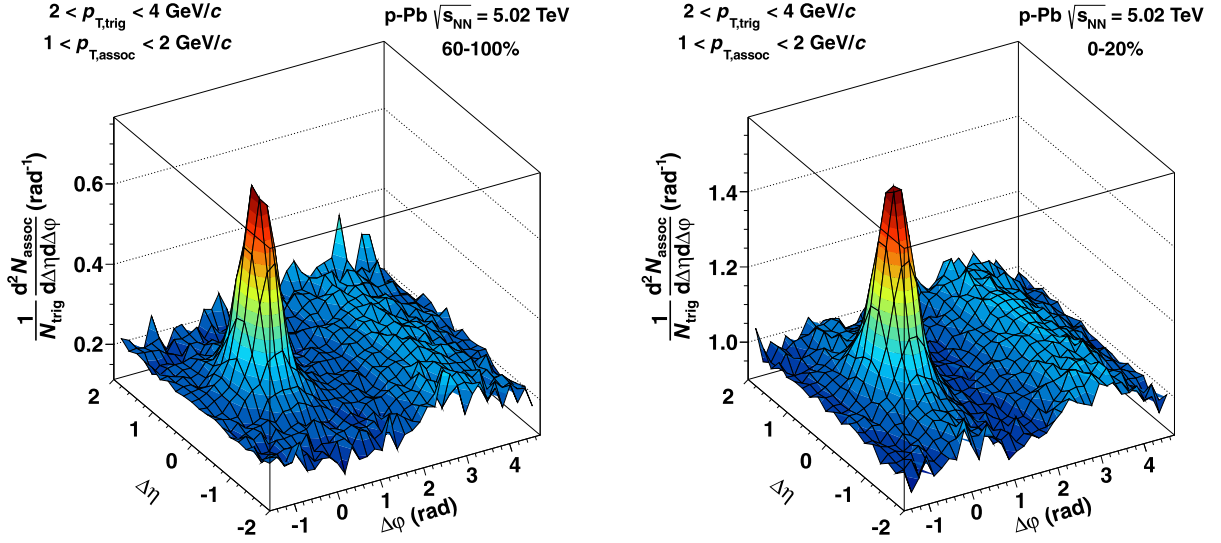
Fig. 1. The associated yield per trigger particle in $\Delta\varphi$ and $\Delta\eta$ for pairs of charged particles with $2 < p_{T,trig} < 4$ GeV/c and $1 < p_{T,assoc} < 2$ GeV/c in p–Pb collisions at $\sqrt{s_{NN}} = 5.02$ TeV for the 60–100% (left) and 0–20% (right) event classes.

different intervals of trigger and associated transverse momentum, $p_{T,trig}$ and $p_{T,assoc}$, respectively, and $p_{T,assoc} < p_{T,trig}$. The associated yield per trigger particle is defined as

$$\frac{1}{N_{trig}} \frac{d^2 N_{assoc}}{d\Delta\eta \, d\Delta\varphi} = \frac{S(\Delta\eta, \Delta\varphi)}{B(\Delta\eta, \Delta\varphi)} \qquad (1)$$

where N_{trig} is the total number of trigger particles in the event class and $p_{T,trig}$ interval. The signal distribution $S(\Delta\eta, \Delta\varphi) = 1/N_{trig} \, d^2 N_{same}/d\Delta\eta \, d\Delta\varphi$ is the associated yield per trigger particle for particle pairs from the same event. In a given event class and p_T interval, the sum over the events is performed separately for N_{trig} and $d^2 N_{same}/d\Delta\eta \, d\Delta\varphi$ before their ratio is computed. Note, that this definition is different from the one used in Ref. [22], where $S(\Delta\eta, \Delta\varphi)$ is calculated per event and then averaged. The method used in this Letter does not induce an inherent multiplicity dependence in the pair yields, which is important for the subtraction method discussed in the next section. The background distribution $B(\Delta\eta, \Delta\varphi) = \alpha \, d^2 N_{mixed}/d\Delta\eta \, d\Delta\varphi$ corrects for pair acceptance and pair efficiency. It is constructed by correlating the trigger particles in one event with the associated particles from other events in the same event class and within the same 2 cm wide z_{vtx} interval (each event is mixed with 5–20 events). The factor α is chosen to normalize the background distribution such that it is unity for pairs where both particles go into approximately the same direction (i.e. $\Delta\varphi \approx 0$, $\Delta\eta \approx 0$). To account for different pair acceptance and pair efficiency as a function of z_{vtx}, the yield defined by Eq. (1) is constructed for each z_{vtx} interval. The final per-trigger yield is obtained by calculating the weighted average of the z_{vtx} intervals.

When constructing the signal and background distributions, the trigger and associated particles are required to be separated by $|\Delta\varphi^*_{min}| > 0.02$ and $|\Delta\eta| > 0.02$, where $\Delta\varphi^*_{min}$ is the minimal azimuthal distance at the same radius between the two tracks within the active detector volume after accounting for the bending due to the magnetic field. This procedure is applied to avoid a bias due to the reduced efficiency for pairs with small opening angles and leads to an increase in the associated near-side peak yield of 0.4–0.8% depending on p_T. Furthermore, particle pairs are removed which are likely to stem from a γ-conversion, or a K_s^0 or Λ decay, by a cut on the invariant mass of the pair (the electron, pion, or

pion/proton mass is assumed, respectively). The effect on the near-side peak yields is less than 2%.

In the signal as well as in the background distribution, each trigger and each associated particle is weighted with a correction factor that accounts for detector acceptance, reconstruction efficiency and contamination by secondary particles. These corrections are applied as a function of η, p_T and z_{vtx}. Applying the correction factors extracted from DPMJET simulations to events simulated with HIJING [50] leads to associated peak yields that agree within 4% with the MC truth. This difference between the two-dimensional corrected per-trigger yield and input per-trigger yield is used in the estimate of the systematic uncertainties. Uncertainties due to track-quality cuts are evaluated by comparing the results of two different track selections, see Section 3. The associated yields are found to be insensitive to these track selections within 5%. Further systematic uncertainties related to specific observables are mentioned below.

5. Results

The associated yield per trigger particle in $\Delta\varphi$ and $\Delta\eta$ is shown in Fig. 1 for pairs of charged particles with $2 < p_{T,trig} < 4$ GeV/c and $1 < p_{T,assoc} < 2$ GeV/c in p–Pb collisions at $\sqrt{s_{NN}} = 5.02$ TeV in the 60–100% (left) and 0–20% (right) event classes. In the 60–100% class, the visible features are the correlation peak near ($\Delta\varphi \approx 0$, $\Delta\eta \approx 0$) for pairs of particles originating from the same jet, and the elongated structure at $\Delta\varphi \approx \pi$ for pairs of particles back-to-back in azimuth. These are similar to those observed in pp collisions at $\sqrt{s} = 2.76$ and 7 TeV. The same features are visible in the 0–20% class. However, both the yields on the near side ($|\Delta\varphi| < \pi/2$) and the away side ($\pi/2 < \Delta\varphi < 3\pi/2$) are higher.[1] This is illustrated in Fig. 2, where the projections on $\Delta\varphi$ averaged over $|\Delta\eta| < 1.8$ are compared for different event classes and also compared to pp collisions at 2.76 and 7 TeV. In order to facilitate the comparison, the yield at $\Delta\varphi = 1.3$ has been subtracted for each distribution. It is seen that the per-trigger yields in $\Delta\varphi$ on the near side and on the away side are similar for low-multiplicity

---

[1] These definitions of near-side ($|\Delta\varphi| < \pi/2$) and away-side ($\pi/2 < \Delta\varphi < 3\pi/2$) are used throughout the Letter.
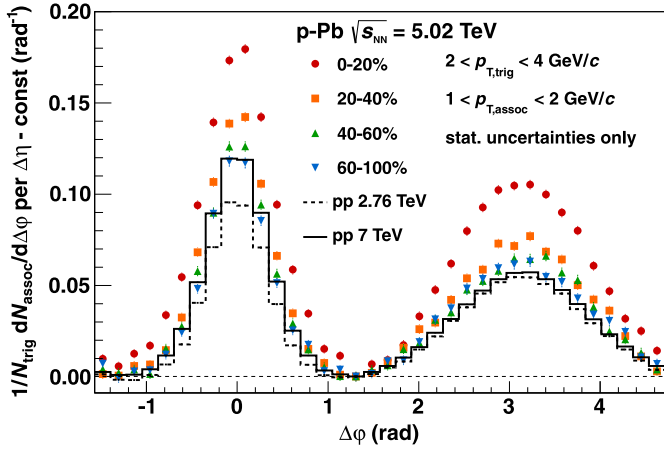
Fig. 2. Associated yield per trigger particle as a function of $\Delta\varphi$ averaged over $|\Delta\eta| <$ 1.8 for pairs of charged particles with $2 < p_{T,trig} < 4$ GeV/c and $1 < p_{T,assoc} <$ 2 GeV/c in p–Pb collisions at $\sqrt{s_{NN}} = 5.02$ TeV for different event classes, and in pp collisions at 2.76 and 7 TeV. The yield between the peaks (determined at $\Delta\varphi \approx 1.3$) has been subtracted in each case. Only statistical uncertainties are shown; systematic uncertainties are less than 0.01 (absolute) per bin.

p–Pb collisions and for pp collisions at $\sqrt{s} = 7$ TeV, and increase with increasing multiplicity in p–Pb collisions.

To quantify the change from low to high multiplicity event classes, we subtract the per-trigger yield of the lowest (60–100%) from that of the higher multiplicity classes. The resulting distribution in $\Delta\varphi$ and $\Delta\eta$ for the 0–20% event class is shown in Fig. 3 (left). A distinct excess structure in the correlation is observed, which forms two ridges, one on the near side and one on the away side. The ridge on the near side is qualitatively similar to the one recently reported by the CMS Collaboration [22]. Note, however that a quantitative comparison would not be meaningful due to the different definition of the per-trigger yield and the different detector acceptance and event-class definition.

On the near side, there is a peak around ($\Delta\varphi \approx 0$, $\Delta\eta \approx 0$) indicating a small change of the near-side jet yield as a function of multiplicity. The integral of this peak above the ridge within $|\Delta\eta| < 0.5$ corresponds to about 5–25% of the unsubtracted near-side peak yield, depending on p_T. In order to avoid a bias on the associated yields due to the multiplicity selection and to prevent that this remaining peak contributes to the ridge yields calculated below, the region $|\Delta\eta| < 0.8$ on the near side is excluded when performing projections onto $\Delta\varphi$. The effect of this incomplete
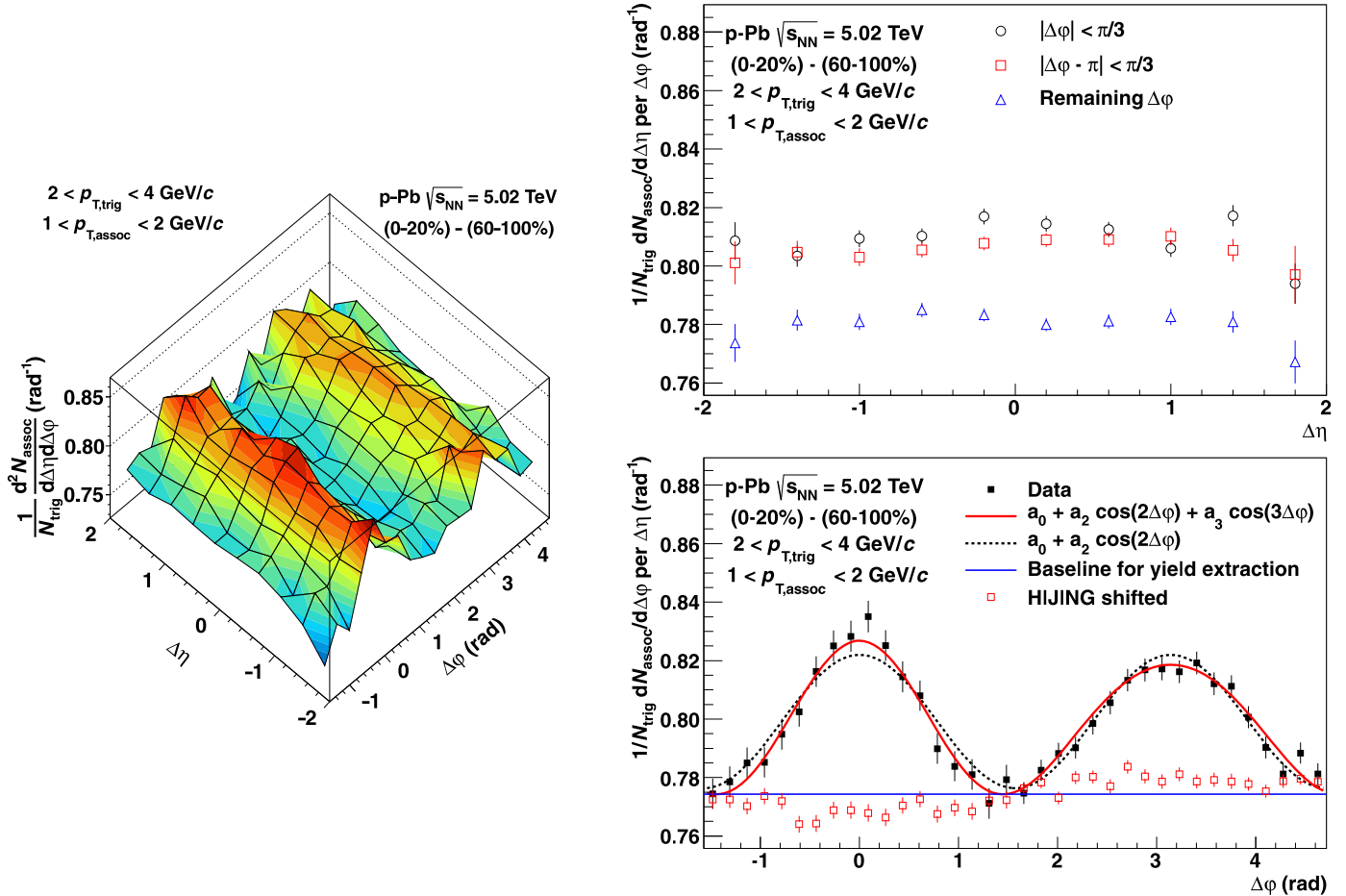

Fig. 3. Left: Associated yield per trigger particle in $\Delta\varphi$ and $\Delta\eta$ for pairs of charged particles with $2 < p_{T,trig} < 4$ GeV/c and $1 < p_{T,assoc} < 2$ GeV/c in p–Pb collisions at $\sqrt{s_{NN}} = 5.02$ TeV for the 0–20% multiplicity class, after subtraction of the associated yield obtained in the 60–100% event class. Top right: the associated per-trigger yield after subtraction (as shown on the left) projected onto $\Delta\eta$ averaged over $|\Delta\varphi| < \pi/3$ (black circles), $|\Delta\varphi - \pi| < \pi/3$ (red squares), and the remaining area (blue triangles, $\Delta\varphi < -\pi/3$, $\pi/3 < \Delta\varphi < 2\pi/3$ and $\Delta\varphi > 4\pi/3$). Bottom right: as above but projected onto $\Delta\varphi$ averaged over $0.8 < |\Delta\eta| < 1.8$ on the near side and $|\Delta\eta| < 1.8$ on the away side. Superimposed are fits containing a $\cos(2\Delta\varphi)$ shape alone (black dashed line) and a combination of $\cos(2\Delta\varphi)$ and $\cos(3\Delta\varphi)$ shapes (red solid line). The blue horizontal line shows the baseline obtained from the latter fit which is used for the yield calculation. Also shown for comparison is the subtracted associated yield when the same procedure is applied on HIJING shifted to the same baseline. The figure shows only statistical uncertainties. Systematic uncertainties are mostly correlated and affect the baseline. Uncorrelated uncertainties are less than 1%. (For interpretation of the references to colour in this figure legend, the reader is referred to the web version of this Letter.)
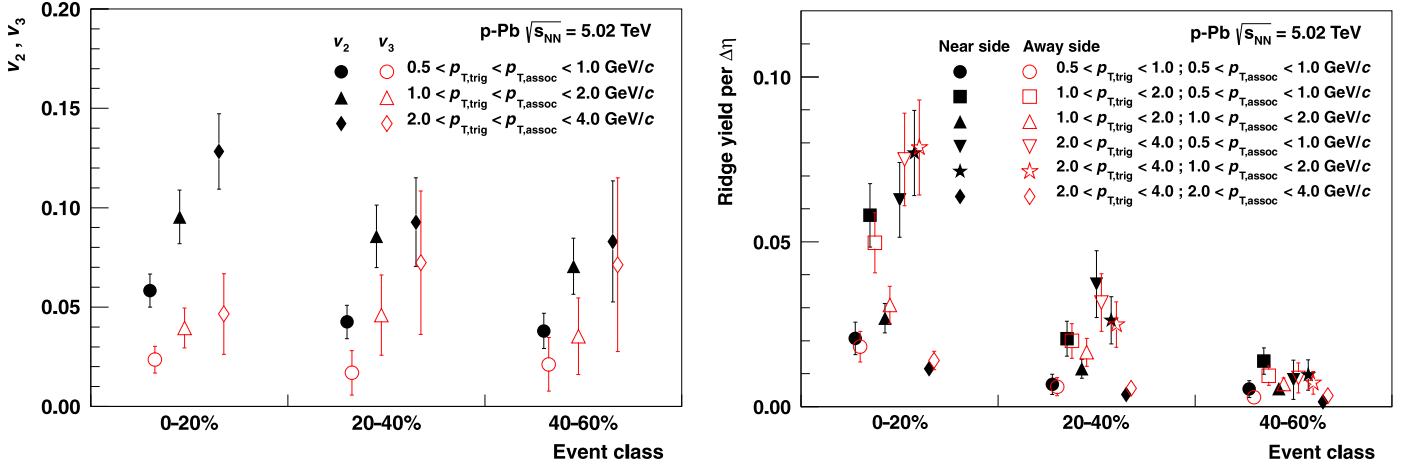
Fig. 4. Left: v_2 (black closed symbols) and v_3 (red open symbols) for different multiplicity classes and overlapping $p_{T,\text{assoc}}$ and $p_{T,\text{trig}}$ intervals. Right: Near-side (black closed symbols) and away-side (red open symbols) ridge yields per unit of $\Delta\eta$ for different $p_{T,\text{trig}}$ and $p_{T,\text{assoc}}$ bins as a function of the multiplicity class. The error bars show statistical and systematic uncertainties added in quadrature. In both panels the points are slightly displaced horizontally for visibility. (For interpretation of the references to colour in this figure legend, the reader is referred to the web version of this Letter.)

subtraction on the extracted observables, which if jet-related might also be present on the away side, is discussed further below.

The top right panel in Fig. 3 shows the projection of Fig. 3 (left) onto $\Delta\eta$ averaged over different $\Delta\varphi$ intervals. The near-side and away-side distributions are flat apart from the discussed small peak around $\Delta\eta = 0$. The bottom right panel shows the projection to $\Delta\varphi$, where a modulation is observed. For comparison, the subtracted associated yield for HIJING simulated events shifted to the baseline of the data is also shown, where no significant modulation remains. To quantify the near-side and away-side excess structures, the following functional form

$$1/N_{\text{trig}} \, dN_{\text{assoc}}/d\Delta\varphi = a_0 + 2a_2 \cos(2\Delta\varphi) + 2a_3 \cos(3\Delta\varphi) \quad (2)$$

is fit to the data in multiplicity and p_T intervals. The fits have a χ^2/ndf of less than 1.5 with and less than 1.8 without the $a_3 \cos(3\Delta\varphi)$ term in the different p_T and multiplicity intervals, indicating that the data are well described by the fits. An example for the fit with and without the $a_3 \cos(3\Delta\varphi)$ term is shown in the bottom right panel of Fig. 3. The fit parameters a_2 and a_3 are a measure of the absolute modulation in the subtracted per-trigger yield and characterize a modulation relative to the baseline b in the higher multiplicity class assuming that such a modulation is not present in the 60–100% event class. This assumption has been checked by subtracting the yields obtained in $\sqrt{s} = 2.76$ and 7 TeV pp collisions from the yields obtained for the 60–100% p–Pb event class and verifying that in both cases no significant signal remains. Therefore, the Fourier coefficients v_n of the corresponding single-particle distribution, commonly used in the analysis of particle correlations in nucleus–nucleus collisions [15], can be obtained in bins where the $p_{T,\text{trig}}$ and $p_{T,\text{assoc}}$ intervals are identical using

$$v_n = \sqrt{a_n/b}. \quad (3)$$

The baseline b is evaluated in the higher-multiplicity class in the region $|\Delta\varphi - \pi/2| < 0.2$, corrected for the fact that it is obtained in the minimum of Eq. (2). A potential bias due to the above-mentioned incomplete near-side peak subtraction on v_2 and v_3 is evaluated in the following way: (a) the size of the near-side exclusion region is changed from $|\Delta\eta| < 0.8$ to $|\Delta\eta| < 1.2$; (b) the residual near-side peak above the ridge is also subtracted from the away side by mirroring it at $\Delta\varphi = \pi/2$ accounting for the general p_T-dependent difference of near-side and away-side jet yields due to the kinematic constraints and the detector acceptance, which

is evaluated using the lowest multiplicity class; and c) the lower multiplicity class is scaled before the subtraction such that no residual near-side peak above the ridge remains. The resulting differences in v_2 (up to 15%) and v_3 coefficients (up to 40%) when applying these approaches have been added to the systematic uncertainties.

The coefficients v_2 and v_3 are shown in the left panel of Fig. 4 for different event classes. The coefficient v_2 increases with increasing p_T, and shows only a small dependence on multiplicity. In the 0–20% event class, v_2 increases from 0.06 ± 0.01 for $0.5 < p_T < 1$ GeV/c to 0.12 ± 0.02 for $2 < p_T < 4$ GeV/c, while v_3 is about 0.03 and shows, within large errors, an increasing trend with p_T. Ref. [34] gives predictions for two-particle correlations arising from collective flow in p–Pb collisions at the LHC in the framework of a hydrodynamical model. The values for v_2 and v_3 coefficients, as well as the p_T and the multiplicity dependences, are in qualitative agreement with the presented results.

To extract information on the yields and widths of the excess distributions in Fig. 3 (bottom right), a constant baseline assuming zero yield at the minimum of the fit function (Eq. (2)) is subtracted. The remaining yield is integrated on the near side and on the away side. Alternatively, a baseline evaluated from the minimum of a parabolic function fitted within $|\Delta\varphi - \pi/2| < 1$ is used; the difference on the extracted yields is added to the systematic uncertainties. The uncertainty imposed by the residual near-side jet peak on the yield is evaluated in the same way as for the v_n coefficients. The near-side and away-side ridge yields are shown in the right panel of Fig. 4 for different event classes and for different combinations of $p_{T,\text{trig}}$ and $p_{T,\text{assoc}}$ intervals. The near-side and away-side yields range from 0 to 0.08 per unit of $\Delta\eta$ depending on multiplicity class and p_T interval. It is remarkable that the near-side and away-side yields always agree within uncertainties for a given sample despite the fact that the absolute values change substantially with event class and p_T interval. Such a tight correlation between the yields is non-trivial and suggests a common underlying physical origin for the near-side and the away-side ridges.

From the baseline-subtracted per-trigger yields the square root of the variance, σ, within $|\Delta\varphi| < \pi/2$ and $\pi/2 < \Delta\varphi < 3\pi/2$ for the near-side and away-side region, respectively, is calculated. The extracted widths on the near side and the away side agree with each other within 20% and vary between 0.5 and 0.7. There is no significant p_T dependence, which suggests that the observed ridge is not of jet origin.
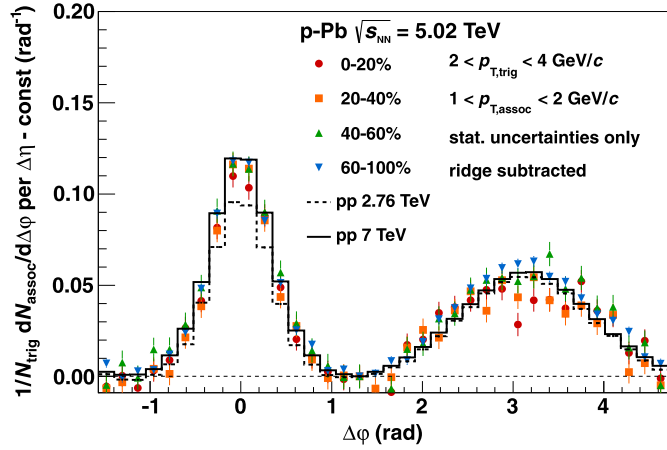
Fig. 5. Associated yield per trigger particle as a function of $\Delta\varphi$ averaged over $|\Delta\eta| < 1.8$ for pairs of charged particles with $2 < p_{T,trig} < 4$ GeV/c and $1 < p_{T,assoc} < 2$ GeV/c in p–Pb collisions at $\sqrt{s_{NN}} = 5.02$ TeV for different event classes, compared to pp collisions at $\sqrt{s} = 2.76$ and 7 TeV. For the event classes 0–20%, 20–40% and 40–60% the long-range contribution on the near-side $1.2 < |\Delta\eta| < 1.8$ and $|\Delta\varphi| < \pi/2$ has been subtracted from both the near side and the away side as described in the text. Subsequently, the yield between the peaks (determined at $\Delta\varphi \approx 1.3$) has been subtracted in each case. Only statistical uncertainties are shown; systematic uncertainties are less than 0.01 (absolute) per bin.

The analysis has been repeated using the forward ZNA detector instead of the VZERO for the definition of the event classes. Unlike in nucleus–nucleus collisions, the correlation between forward energy measured in the ZNA and particle density at central rapidities is very weak in proton–nucleus collisions. Therefore, event classes defined as fixed fractions of the signal distribution in the ZNA select different events, with different mean particle multiplicity at midrapidity, than the samples selected with the same fractions in the VZERO detector. While the event classes selected with the ZNA span a much smaller range in central multiplicity density, they also minimize any autocorrelation between multiplicity selections and, for example, jet activity. With the ZNA selection, we find qualitatively consistent results compared to the VZERO selection. In particular, an excess in the difference between low-multiplicity and high-multiplicity ZNA selected events is observed to be symmetric on the near side and away side. Also, the v_n coefficients and σ widths are similar within uncertainties. However, both the ridge yields and mean charged-particle multiplicity density at midrapidity are different between the VZERO and ZNA event classes. Nevertheless, within the uncertainties, both follow a common trend as a function of $\langle dN_{ch}/d\eta \rangle|_{|\eta|<0.5}$.

So far it has been seen that the assumption of an unmodified jet shape in different multiplicity classes in p–Pb collisions resulted in the emergence of almost identical ridge-like excess structures on the near-side and away side, most pronounced in high-multiplicity events. An alternative approach is to start with the assumption that there are identical ridge structures on the near side and away side, and to study whether this assumption leaves any room for multiplicity dependent modifications of the jet shape, in particular on the away side. To this end, a symmetric ridge structure is subtracted on the near side and away side from the $\Delta\varphi$ projection of the associated yield per trigger averaged over $|\Delta\eta| < 1.8$. The near-side ridge structure is determined in the same event class within $1.2 < |\Delta\eta| < 1.8$, while the ridge on the away side is constructed by mirroring this near-side structure at $\Delta\varphi = \pi/2$. The ridge-subtracted results in the interval $2 < p_{T,trig} < 4$ GeV/c and $1 < p_{T,assoc} < 2$ GeV/c for the 0–20%, 20–40% and 40–60% event classes are shown in Fig. 5 compared

to the unsubtracted 60–100% event class and to pp collisions. The remaining yields in all event classes are in agreement with each other and with pp collisions, indicating that the observed correlations are indeed consistent with a symmetric ridge and with no further significant modification of the jet structure at midrapidity in high-multiplicity p–Pb collisions at the LHC, in contrast to what was seen at forward rapidity in $\sqrt{s_{NN}} = 0.2$ TeV d–Au collisions at RHIC [36].

6. Summary

Results from angular correlations between charged trigger and associated particles in p–Pb collisions at $\sqrt{s_{NN}} = 5.02$ TeV are presented for various transverse momentum ranges within $0.5 < p_{T,assoc} < p_{T,trig} < 4$ GeV/c. Associated yields per trigger particle are measured over two units of pseudorapidity and full azimuthal angle in different multiplicity classes. The yields projected onto $\Delta\varphi$ increase with event multiplicity and rise to values higher than those observed in pp collisions at $\sqrt{s} = 2.76$ and 7 TeV. The difference between the yields per trigger particle in high-multiplicity and low-multiplicity events exhibits two nearly identical, long-range (up to $|\Delta\eta| \sim 2$) ridge-like excess structures on the near-side ($\Delta\varphi \approx 0$) and away-side ($\Delta\varphi \approx \pi$) as quantified by their yields and widths. The excess on the near side at high event multiplicity is qualitatively similar to that recently reported by the CMS Collaboration in $2 < |\Delta\eta| < 4$ [22]. The excess on the away side with respect to the usual away-side structure due to back-to-back jets and momentum conservation is reported here for the first time, and confirmed by a similar study from the ATLAS Collaboration [51] that appeared after publication of this Letter. The event multiplicity and p_T dependences of the near-side and away-side ridge yields are in good agreement, and their widths show no significant dependence on multiplicity or p_T. The observation of a nearly identical near-side and away-side ridge-like structure is consistent with Colour Glass Condensate model calculations [25]. At the same time, the extracted v_2 and v_3 coefficients are in qualitative agreement with a hydrodynamical model calculation [35]. Further theoretical investigation is needed for a detailed understanding of the origin of these long-range correlation structures. After subtracting the near-side ridge from the near side and away side symmetrically, the correlation shape in $\Delta\varphi$ becomes independent of multiplicity and similar to those of pp collisions at 7 TeV. There is no evidence in the present data for further significant structures in two-particle correlations at midrapidity in p–Pb collisions at $\sqrt{s_{NN}} = 5.02$ TeV.

References

[1] X.-N. Wang, Phys. Rev. D 47 (1993) 2754.
[2] J. Adams, et al., Phys. Rev. C 73 (2006) 064907.
[3] B. Alver, et al., Phys. Rev. C 81 (2010) 024904.
[4] B. Alver, et al., Phys. Rev. Lett. 104 (2010) 062301.
[5] B.I. Abelev, et al., Phys. Rev. C 80 (2009) 064912.
[6] S. Chatrchyan, et al., JHEP 1107 (2011) 076.
[7] K. Aamodt, et al., Phys. Lett. B 708 (2012) 249.
[8] G. Agakishiev, et al., Anomalous centrality evolution of two-particle angular correlations from Au-Au collisions at $\sqrt{s_{NN}} = 62$ and 200 GeV, arXiv:1109.4380 [nucl-ex], 2011.
[9] S. Chatrchyan, et al., Eur. Phys. J. C 72 (2012) 2012.
[10] G. Aad, et al., Phys. Rev. C 86 (2012) 014907.
[11] K. Aamodt, et al., Phys. Rev. Lett. 107 (2011) 032301.
[12] A. Adare, et al., Phys. Rev. Lett. 107 (2011) 252301.
[13] B. Abelev, et al., Anisotropic flow of charged hadrons, pions and (anti-)protons measured at high transverse momentum in Pb-Pb collisions at $\sqrt{s_{NN}} = 2.76$ TeV, arXiv:1205.5761 [nucl-ex], 2012.
[14] S. Chatrchyan, et al., Measurement of the azimuthal anisotropy of neutral pions in Pb–Pb collisions at $\sqrt{s_{NN}} = 2.76$ TeV, arXiv:1208.2470 [nucl-ex], 2012.
[15] S. Voloshin, Y. Zhang, Z. Phys. C 70 (1996) 665.
[16] J.-Y. Ollitrault, Phys. Rev. D 46 (1992) 229.
[17] B. Alver, G. Roland, Phys. Rev. C 81 (2010) 054905.
[18] B. Alver, C. Gombeaud, M. Luzum, J.-Y. Ollitrault, Phys. Rev. C 82 (2010) 034913.
[19] B. Schenke, S. Jeon, C. Gale, Phys. Rev. Lett. 106 (2011) 042301.
[20] Z. Qiu, C. Shen, U. Heinz, Phys. Lett. B 707 (2012) 151.
[21] V. Khachatryan, et al., JHEP 1009 (2010) 091.
[22] S. Chatrchyan, et al., Observation of long-range near-side angular correlations in proton–lead collisions at the LHC, arXiv:1210.5482 [nucl-ex], 2012.
[23] B. Arbuzov, E. Boos, V. Savrin, Eur. Phys. J. C 71 (2011) 1730.
[24] K. Dusling, R. Venugopalan, Evidence for BFKL and saturation dynamics from di-hadron spectra at the LHC, arXiv:1210.3890 [hep-ph], 2012.
[25] K. Dusling, R. Venugopalan, Explanation of systematics of CMS p–Pb high multiplicity di-hadron data at $\sqrt{s_{NN}} = 5.02$ TeV, arXiv:1211.3701 [hep-ph], 2012.
[26] Y.V. Kovchegov, D.E. Wertepny, Long-range rapidity correlations in heavy–light ion collisions, arXiv:1212.1195 [hep-ph], 2012.
[27] C.-Y. Wong, Phys. Rev. C 84 (2011) 024901.
[28] M. Strikman, Acta Phys. Polon. B 42 (2011) 2607.
[29] S. Alderweireldt, P. Van Mechelen, Obtaining the CMS ridge effect with multiparton interactions, arXiv:1203.2048 [hep-ph], 2012.
[30] E. Avsar, C. Flensburg, Y. Hatta, J.-Y. Ollitrault, T. Ueda, Phys. Lett. B 702 (2011) 394.
[31] K. Werner, I. Karpenko, T. Pierog, Phys. Rev. Lett. 106 (2011) 122004.
[32] W.-T. Deng, Z. Xu, C. Greiner, Phys. Lett. B 711 (2012) 301.
[33] E. Avsar, Y. Hatta, C. Flensburg, J. Ollitrault, T. Ueda, J. Phys. G 38 (2011) 124053.
[34] P. Bozek, Phys. Rev. C 85 (2012) 014911.
[35] P. Bozek, W. Broniowski, Correlations from hydrodynamic flow in p–Pb collisions, arXiv:1211.0845 [nucl-th], 2012.
[36] E. Braidot, Suppression of forward pion correlations in d–Au interactions at STAR, arXiv:1005.2378 [hep-ph], 2010.
[37] A. Adare, et al., Phys. Rev. Lett. 107 (2011) 172301.
[38] J.L. Albacete, C. Marquet, Phys. Rev. Lett. 105 (2010) 162301.
[39] K. Aamodt, et al., JINST 3 (2008) S08002.
[40] K. Aamodt, et al., Eur. Phys. J. C 68 (2010) 89.
[41] B. Abelev, et al., Pseudorapidity density of charged particles in p–Pb collisions at $\sqrt{s_{NN}} = 5.02$ TeV, arXiv:1210.3615 [nucl-ex], 2012.
[42] B. Abelev, et al., Centrality dependence of charged particle production at large transverse momentum in Pb–Pb collisions at $\sqrt{s_{NN}} = 2.76$ TeV, arXiv:1208.2711 [hep-ex], 2012.
[43] B. Abelev, et al., Performance of the ALICE at the LHC (2013), in preparation.
[44] B. Abelev, et al., JHEP 1203 (2012) 053.
[45] B. Abelev, et al., JHEP 1207 (2012) 116.
[46] S. Roesler, R. Engel, J. Ranft, The Monte Carlo event generator DPMJET-III, arXiv:hep-ph/0012252, 2000.
[47] T. Sjostrand, S. Mrenna, P.Z. Skands, JHEP 0605 (2006) 026.
[48] P.Z. Skands, Phys. Rev. D 82 (2010) 074018.
[49] R. Brun, et al., CERN Program Library Long Write-up W5013 (1994).
[50] X.-N. Wang, M. Gyulassy, Phys. Rev. D 44 (1991) 3501.
[51] G. Aad, et al., Observation of associated near-side and away-side long-range correlations in $\sqrt{s_{NN}} = 5.02$ TeV proton–lead collisions with the ATLAS detector, arXiv:1212.5198 [hep-ex], 2012.

ALICE Collaboration

Betty Abelev [bs], Jaroslav Adam [ak], Dagmar Adamova [ca], Andrew Marshall Adare [dx], Madan Aggarwal [ce], Gianluca Aglieri Rinella [ag], Michelangelo Agnello [cy,ck], Andras Gabor Agocs [dw], Andrea Agostinelli [aa], Zubayer Ahammed [ds], Nazeer Ahmad [q], Arshad Ahmad [q], Sul-Ah Ahn [bl], Sang Un Ahn [an,bl], Muhammad Ajaz [o], Alexander Akindinov [ax], Dmitry Aleksandrov [cq], Bruno Alessandro [cy], Andrea Alici [cu,l], Anton Alkin [c], Erick Jonathan Almaraz Avina [bh], Johan Alme [ai], Torsten Alt [am], Valerio Altini [ae], Sedat Altinpinar [r], Igor Altsybeev [dt], Cristian Andrei [bw], Anton Andronic [cn], Venelin Anguelov [cj], Jonas Anielski [bf], Christopher Daniel Anson [s], Tome Anticic [co], Federico Antinori [cv], Pietro Antonioli [cu], Laurent Bernard Aphecetche [dd], Harald Appelshauser [bd], Nicolas Arbor [bo], Silvia Arcelli [aa], Andreas Arend [bd], Nestor Armesto [p], Roberta Arnaldi [cy], Tomas Robert Aronsson [dx], Ionut Cristian Arsene [cn], Mesut Arslandok [bd], Andzhey Asryan [dt], Andre Augustinus [ag], Ralf Peter Averbeck [cn], Terry Awes [cb], Juha Heikki Aysto [ap], Mohd Danish Azmi [q,cg],

Matthias Jakob Bach [am], Angela Badala [db], Yong Wook Baek [bn,an], Raphaelle Marie Bailhache [bd], Renu Bala [ch,cy], Rinaldo Baldini Ferroli [l], Alberto Baldisseri [n], Fernando Baltasar Dos Santos Pedrosa [ag], Jaroslav Ban [ay], Rama Chandra Baral [az], Roberto Barbera [z], Francesco Barile [ae], Gergely Gabor Barnafoldi [dw], Lee Stuart Barnby [cs], Valerie Barret [bn], Jerzy Gustaw Bartke [dg], Maurizio Basile [aa], Nicole Bastid [bn], Sumit Basu [ds], Bastian Bathen [bf], Guillaume Batigne [dd], Boris Batyunya [bj], Christoph Heinrich Baumann [bd], Ian Gardner Bearden [by], Hans Beck [bd], Nirbhay Kumar Behera [ar], Iouri Belikov [bi], Francesca Bellini [aa], Rene Bellwied [dm], Ernesto Belmont-Moreno [bh], Gyula Bencedi [dw], Stefania Beole [v], Ionela Berceanu [bw], Alexandru Bercuci [bw], Yaroslav Berdnikov [cc], Daniel Berenyi [dw], Anais Annick Erica Bergognon [dd], Dario Berzano [v,cy], Latchezar Betev [ag], Anju Bhasin [ch], Ashok Kumar Bhati [ce], Jihyun Bhom [dq], Livio Bianchi [v], Nicola Bianchi [bp], Jaroslav Bielcik [ak], Jana Bielcikova [ca], Ante Bilandzic [by], Sandro Bjelogrlic [aw], Francesco Blanco [dm], F. Blanco [j], Dmitry Blau [cq], Christoph Blume [bd], Marco Boccioli [ag], Stefan Boettger [bc], Alexey Bogdanov [bt], Hans Boggild [by], Mikhail Bogolyubsky [au], Laszlo Boldizsar [dw], Marek Bombara [al], Julian Book [bd], Herve Borel [n], Alexander Borissov [dv], Francesco Bossu [cg], Michiel Botje [bz], Elena Botta [v], Ermes Braidot [br], Peter Braun-Munzinger [cn], Marco Bregant [dd], Timo Gunther Breitner [bc], Theo Alexander Broker [bd], Tyler Allen Browning [cl], Michal Broz [aj], Rene Brun [ag], Elena Bruna [v,cy], Giuseppe Eugenio Bruno [ae], Dmitry Budnikov [cp], Henner Buesching [bd], Stefania Bufalino [v,cy], Predrag Buncic [ag], Oliver Busch [cj], Edith Zinhle Buthelezi [cg], Diego Caballero Orduna [dx], Davide Caffarri [ab,cv], Xu Cai [g], Helen Louise Caines [dx], Ernesto Calvo Villar [ct], Paolo Camerini [x], Veronica Canoa Roman [k], Giovanni Cara Romeo [cu], Wisla Carena [ag], Francesco Carena [ag], Nelson Carlin Filho [dj], Federico Carminati [ag], Amaya Ofelia Casanova Diaz [bp], Javier Ernesto Castillo Castellanos [n], Juan Francisco Castillo Hernandez [cn], Ester Anna Rita Casula [w], Vasile Catanescu [bw], Costanza Cavicchioli [ag], Cesar Ceballos Sanchez [i], Jan Cepila [ak], Piergiaio Cerello [cy], Beomsu Chang [ap,dz], Sylvain Chapeland [ag], Jean-Luc Fernand Charvet [n], Sukalyan Chattopadhyay [cr], Subhasis Chattopadhyay [ds], Isha Chawla [ce], Michael Gerard Cherney [cd], Cvetan Cheshkov [ag,dl], Brigitte Cheynis [dl], Vasco Miguel Chibante Barroso [ag], David Chinellato [dm], Peter Chochula [ag], Marek Chojnacki [by,aw], Subikash Choudhury [ds], Panagiotis Christakoglou [bz], Christian Holm Christensen [by], Peter Christiansen [af], Tatsuya Chujo [dq], Suh-Urk Chung [cm], Corrado Cicalo [cx], Luisa Cifarelli [aa,ag,l], Federico Cindolo [cu], Jean Willy Andre Cleymans [cg], Fabrizio Coccetti [l], Fabio Colamaria [ae], Domenico Colella [ae], Alberto Collu [w], Gustavo Conesa Balbastre [bo], Zaida Conesa del Valle [ag], Megan Elizabeth Connors [dx], Giacomo Contin [x], Jesus Guillermo Contreras [k], Thomas Michael Cormier [dv], Yasser Corrales Morales [v], Pietro Cortese [ad], Ismael Cortes Maldonado [b], Mauro Rogerio Cosentino [br], Filippo Costa [ag], Manuel Enrique Cotallo [j], Elisabetta Crescio [k], Philippe Crochet [bn], Emilia Cruz Alaniz [bh], Rigoberto Cruz Albino [k], Eleazar Cuautle [bg], Leticia Cunqueiro [bp], Andrea Dainese [ab,cv], Hans Hjersing Dalsgaard [by], Andrea Danu [bb], Indranil Das [at], Debasish Das [cr], Supriya Das [d], Kushal Das [cr], Ajay Kumar Dash [dk], Sadhana Dash [ar], Sudipan De [ds], Gabriel de Barros [dj], Annalisa De Caro [ac,l], Giacinto de Cataldo [da], Jan de Cuveland [am], Alessandro De Falco [w], Daniele De Gruttola [ac], Hugues Delagrange [dd], Andrzej Deloff [bu], Nora De Marco [cy], Ervin Denes [dw], Salvatore De Pasquale [ac], Airton Deppman [dj], Ginevra D'Erasmo [ae], Raoul Stefan de Rooij [aw], Miguel Angel Diaz Corchero [j], Domenico Di Bari [ae], Thomas Dietel [bf], Carmelo Di Giglio [ae], Sergio Di Liberto [cw], Antonio Di Mauro [ag], Pasquale Di Nezza [bp], Roberto Divia [ag], Oeystein Djuvsland [r], Alexandru Florin Dobrin [dv,af], Tadeusz Antoni Dobrowolski [bu], Benjamin Donigus [cn], Olja Dordic [u], Olga Driga [dd], Anand Kumar Dubey [ds], Andrea Dubla [aw], Laurent Ducroux [dl], Pascal Dupieux [bn], A.K. Dutta Majumdar [cr], Domenico Elia [da], David Philip Emschermann [bf], Heiko Engel [bc], Barbara Erazmus [ag,dd], Hege Austrheim Erdal [ai], Bruno Espagnon [at], Magali Danielle Estienne [dd], Shinichi Esumi [dq], David Evans [cs], Gyulnara Eyyubova [u], Daniela Fabris [ab,cv], Julien Faivre [bo], Davide Falchieri [aa], Alessandra Fantoni [bp], Markus Fasel [cn,cj], Roger Worsley Fearick [cg], Dominik Fehlker [r], Linus Feldkamp [bf], Daniel Felea [bb], Alessandro Feliciello [cy], Bo Fenton-Olsen [br], Grigory Feofilov [dt], Arturo Fernandez Tellez [b], Alessandro Ferretti [v], Andrea Festanti [ab], Jan Figiel [dg], Marcel Figueredo [dj], Sergey Filchagin [cp], Dmitry Finogeev [av], Fiorella Fionda [ae], Enrichetta Maria Fiore [ae], Emmanuel Floratos [cf], Michele Floris [ag], Siegfried Valentin Foertsch [cg], Panagiota Foka [cn], Sergey Fokin [cq], Enrico Fragiacomo [cz], Andrea Francescon [ag,ab], Ulrich Michael Frankenfeld [cn], Ulrich Fuchs [ag], Christophe Furget [bo],

Mario Fusco Girard [ac], Jens Joergen Gaardhoje [by], Martino Gagliardi [v], Alberto Gago [ct], Mauro Gallio [v], Dhevan Raja Gangadharan [s], Paraskevi Ganoti [cb], Jose Garabatos [cn], Edmundo Garcia-Solis [m], Irakli Garishvili [bs], Jochen Gerhard [am], Marie Germain [dd], Claudio Geuna [n], Mihaela Gheata [bb,ag], Andrei Geae Gheata [ag], Bruno Ghidini [ae], Premomoy Ghosh [ds], Paola Gianotti [bp], Martin Robert Girard [du], Paolo Giubellino [ag], Ewa Gladysz-Dziadus [dg], Peter Glassel [cj], Ramon Gomez [di,k], Elena Gonzalez Ferreiro [p], Laura Helena Gonzalez-Trueba [bh], Pedro Gonzalez-Zamora [j], Sergey Gorbunov [am], Ankita Goswami [ci], Sven Gotovac [df], Lukasz Kamil Graczykowski [du], Robert Grajcarek [cj], Alessandro Grelli [aw], Costin Grigoras [ag], Alina Gabriela Grigoras [ag], Vladislav Grigoriev [bt], Ara Grigoryan [a], Smbat Grigoryan [bj], Boris Grinyov [c], Nevio Grion [cz], Philippe Gros [af], Jan Fiete Grosse-Oetringhaus [ag,*], Jean-Yves Grossiord [dl], Raffaele Grosso [ag], Fedor Guber [av], Rachid Guernane [bo], Barbara Guerzoni [aa], Maxime Rene Joseph Guilbaud [dl], Kristjan Herlache Gulbrandsen [by], Hrant Gulkanyan [a], Taku Gunji [dp], Anik Gupta [ch], Ramni Gupta [ch], Rudiger Haake [bf], Oystein Senneset Haaland [r], Cynthia Marie Hadjidakis [at], Maria Haiduc [bb], Hideki Hamagaki [dp], Gergoe Hamar [dw], Byounghee Han [t], Luke David Hanratty [cs], Alexander Hansen [by], Zuzana Harmanova [al], John William Harris [dx], Matthias Hartig [bd], Austin Harton [m], Despoina Hatzifotiadou [cu], Shinichi Hayashi [dp], Arsen Hayrapetyan [ag,a], Stefan Thomas Heckel [bd], Markus Ansgar Heide [bf], Haavard Helstrup [ai], Andrei Ionut Herghelegiu [bw], Gerardo Antonio Herrera Corral [k], Norbert Herrmann [cj], Benjamin Andreas Hess [dr], Kristin Fanebust Hetland [ai], Bernard Hicks [dx], Boris Hippolyte [bi], Yasuto Hori [dp], Peter Zahariev Hristov [ag], Ivana Hrivnacova [at], Meidana Huang [r], Thomas Humanic [s], Dae Sung Hwang [t], Raphaelle Ichou [bn], Radiy Ilkaev [cp], Iryna Ilkiv [bu], Motoi Inaba [dq], Elisa Incani [w], Pier Giaio Innocenti [ag], Gian Michele Innocenti [v], Mikhail Ippolitov [cq], Muhammad Irfan [q], Cristian Geae Ivan [cn], Vladimir Ivanov [cc], Andrey Ivanov [dt], Marian Ivanov [cn], Oleksii Ivanytskyi [c], Adam Wlodzimierz Jacholkowski [z], Peter Jacobs [br], Haeng Jin Jang [bl], Malgorzata Anna Janik [du], Rudolf Janik [aj], Sandun Jayarathna [dm], Satyajit Jena [ar], Deeptanshu Manu Jha [dv], Raul Tonatiuh Jimenez Bustamante [bg], Peter Graham Jones [cs], Hyung Taik Jung [an], Anton Jusko [cs], Alexei Kaidalov [ax], Sebastian Kalcher [am], Peter Kalinak [ay], Tuomo Esa Aukusti Kalliokoski [ap], Alexander Philipp Kalweit [be,ag], Ju Hwan Kang [dz], Vladimir Kaplin [bt], Ayben Karasu Uysal [ag,dy,bm], Oleg Karavichev [av], Tatiana Karavicheva [av], Evgeny Karpechev [av], Andrey Kazantsev [cq], Udo Wolfgang Kebschull [bc], Ralf Keidel [ea], Palash Khan [cr], Shuaib Ahmad Khan [ds], Mohisin Mohammed Khan [q], Kamal Hussain Khan [o], Alexei Khanzadeev [cc], Yury Kharlov [au], Bjarte Kileng [ai], Beomkyu Kim [dz], Jin Sook Kim [an], Jonghyun Kim [t], Dong Jo Kim [ap], Do Won Kim [an,bl], Taesoo Kim [dz], Se Yong Kim [t], Mimae Kim [an], Minwoo Kim [dz], Stefan Kirsch [am], Ivan Kisel [am], Sergey Kiselev [ax], Adam Ryszard Kisiel [du], Jennifer Lynn Klay [f], Jochen Klein [cj], Christian Klein-Bosing [bf], Michael Kliemant [bd], Alexander Kluge [ag], Michael Linus Knichel [cn], Anders Garritt Knospe [dh], Markus Kohler [cn], Thorsten Kollegger [am], Anatoly Kolojvari [dt], Mikhail Kompaniets [dt], Valery Kondratiev [dt], Natalia Kondratyeva [bt], Artem Konevskih [av], Vladimir Kovalenko [dt], Marek Kowalski [dg], Serge Kox [bo], Greeshma Koyithatta Meethaleveedu [ar], Jiri Kral [ap], Ivan Kralik [ay], Frederick Kramer [bd], Adela Kravcakova [al], Tobias Krawutschke [cj,ah], Michal Krelina [ak], Matthias Kretz [am], Marian Krivda [cs,ay], Filip Krizek [ap], Miroslav Krus [ak], Evgeny Kryshen [cc], Mikolaj Krzewicki [cn], Yury Kucheriaev [cq], Thanushan Kugathasan [ag], Christian Claude Kuhn [bi], Paul Kuijer [bz], Igor Kulakov [bd], Jitendra Kumar [ar], Podist Kurashvili [bu], A. Kurepin [av], A.B. Kurepin [av], Alexey Kuryakin [cp], Svetlana Kushpil [ca], Vasily Kushpil [ca], Henning Kvaerno [u], Min Jung Kweon [cj], Youngil Kwon [dz], Pedro Ladron de Guevara [bg], Igor Lakomov [at], Rune Langoy [r], Sarah Louise La Pointe [aw], Camilo Ernesto Lara [bc], Antoine Xavier Lardeux [dd], Paola La Rocca [z], Ramona Lea [x], Mateusz Lechman [ag], Ki Sang Lee [an], Sung Chul Lee [an], Graham Richard Lee [cs], Iosif Legrand [ag], Joerg Walter Lehnert [bd], Matthieu Laurent Lenhardt [cn], Vito Lenti [da], Hermes Leon [bh], Ildefonso Leon Monzon [di], Hermes Leon Vargas [bd], Peter Levai [dw], Shuang Li [g], Jaen Lien [r], Roman Lietava [cs], Svein Lindal [u], Volker Lindenstruth [am], Christian Lippmann [cn,ag], Michael Annan Lisa [s], Hans Martin Ljunggren [af], Per-Ivar Loenne [r], Vera Loggins [dv], Vitaly Loginov [bt], Daniel Lohner [cj], Constantinos Loizides [br], Kai Krister Loo [ap], Xavier Bernard Lopez [bn], Ernesto Lopez Torres [i], Gunnar Lovhoiden [u], Xianguo Lu [cj], Philipp Luettig [bd], Marcello Lunardon [ab], Jiebin Luo [g], Grazia Luparello [aw], Cinzia Luzzi [ag], Rongrong Ma [dx], Ke Ma [g], Dilan Minthaka Madagodahettige-Don [dm], Alla Maevskaya [av], Magnus Mager [be,ag],

Durga Prasad Mahapatra [az], Antonin Maire [cj], Mikhail Malaev [cc], Ivonne Alicia Maldonado Cervantes [bg], Ludmila Malinina [bj,i], Dmitry Mal'Kevich [ax], Peter Malzacher [cn], Alexander Mamonov [cp], Loic Henri Antoine Manceau [cy], Lalit Kumar Mangotra [ch], Vladislav Manko [cq], Franck Manso [bn], Vito Manzari [da], Yaxian Mao [g], Massimiliano Marchisone [bn,v], Jiri Mares [ba], Giacomo Vito Margagliotti [x,cz], Anselmo Margotti [cu], Ana Maria Marin [cn], Christina Markert [dh], Marco Marquard [bd], Irakli Martashvili [do], Nicole Alice Martin [cn], Paolo Martinengo [ag], Mario Ivan Martinez [b], Arnulfo Martinez Davalos [bh], Gines Martinez Garcia [dd], Yevgen Martynov [c], Alexis Jean-Michel Mas [dd], Silvia Masciocchi [cn], Massimo Masera [v], Alberto Masoni [cx], Laure Marie Massacrier [dd], Annalisa Mastroserio [ae], Adam Tomasz Matyja [dg,dd], Christoph Mayer [dg], Joel Mazer [do], Alessandra Maria Mazzoni [cw], Franco Meddi [y], Arturo Alejandro Menchaca-Rocha [bh], Jae Mercado Perez [cj], Michal Meres [aj], Yasuo Miake [dq], Leonardo Milano [v], Jovan Milosevic [u,ii], Andre Mischke [aw], Aditya Nath Mishra [ci,as], Dariusz Miskowiec [cn], Ciprian Mihai Mitu [bb], Sanshiro Mizuno [dq], Jocelyn Mlynarz [dv], Bedangadas Mohanty [ds,bx], Levente Molnar [dw,ag,bi], Luis Manuel Montano Zetina [k], Marco Monteno [cy], Esther Montes [j], Taebong Moon [dz], Maurizio Morando [ab], Denise Aparecida Moreira De Godoy [dj], Sandra Moretto [ab], Astrid Morreale [ap], Andreas Morsch [ag], Valeria Muccifora [bp], Eugen Mudnic [df], Sanjib Muhuri [ds], Maitreyee Mukherjee [ds], Hans Muller [ag], Marcelo Munhoz [dj], Sean Murray [cg], Luciano Musa [ag], Jan Musinsky [ay], Alfredo Musso [cy], Basanta Kumar Nandi [ar], Rosario Nania [cu], Eugenio Nappi [da], Christine Nattrass [do], Tapan Kumar Nayak [ds], Sergey Nazarenko [cp], Alexander Nedosekin [ax], Maria Nicassio [ae,cn], Mihai Niculescu [bb,ag], Bae Svane Nielsen [by], Takafumi Niida [dq], Sergey Nikolaev [cq], Vedran Nikolic [co], Sergey Nikulin [cq], Vladimir Nikulin [cc], Bjorn Steven Nilsen [cd], Mads Stormo Nilsson [u], Francesco Noferini [cu,l], Petr Nomokonov [bj], Gerardus Nooren [aw], Norbert Novitzky [ap], Alexandre Nyanin [cq], Anitha Nyatha [ar], Casper Nygaard [by], Joakim Ingemar Nystrand [r], Alexander Ochirov [dt], Helmut Oskar Oeschler [be,ag], Saehanseul Oh [dx], Sun Kun Oh [an], Janusz Oleniacz [du], Antonio Carlos Oliveira Da Silva [dj], Chiara Oppedisano [cy], Antonio Ortiz Velasquez [af,bg], Anders Nils Erik Oskarsson [af], Piotr Krystian Ostrowski [du], Jacek Tomasz Otwinowski [cn], Ken Oyama [cj], Kyoichiro Ozawa [dp], Yvonne Chiara Pachmayer [cj], Milos Pachr [ak], Fatima Padilla [v], Paola Pagano [ac], Guy Paic [bg], Florian Painke [am], Carlos Pajares [p], Susanta Kumar Pal [ds], Arvinder Singh Palaha [cs], Armando Palmeri [db], Vardanush Papikyan [a], Giuseppe Pappalardo [db], Woo Jin Park [cn], Annika Passfeld [bf], Blahoslav Pastircak [ay], Dmitri Ivanovich Patalakha [au], Vincenzo Paticchio [da], Biswarup Paul [cr], Alexei Pavlinov [dv], Tomasz Jan Pawlak [du], Thomas Peitzmann [aw], Hugo Denis Antonio Pereira Da Costa [n], Elienos Pereira De Oliveira Filho [dj], Dmitri Peresunko [cq], Carlos Eugenio Perez Lara [bz], Diego Perini [ag], Davide Perrino [ae], Wiktor Stanislaw Peryt [du], Alessandro Pesci [cu], Vladimir Peskov [ag,bg], Yury Pestov [e], Vojtech Petracek [ak], Michal Petran [ak], Mariana Petris [bw], Plamen Rumenov Petrov [cs], Mihai Petrovici [bw], Catia Petta [z], Stefano Piano [cz], Miroslav Pikna [aj], Philippe Pillot [dd], Ombretta Pinazza [ag], Lawrence Pinsky [dm], Nora Pitz [bd], Danthasinghe Piyarathna [dm], Mirko Planinic [co], Mateusz Andrzej Ploskon [br], Jan Marian Pluta [du], Timur Pocheptsov [bj], Sona Pochybova [dw], Pedro Luis Manuel Podesta Lerma [di], Martin Poghosyan [ag], Karel Polak [ba], Boris Polichtchouk [au], Amalia Pop [bw], Sarah Porteboeuf-Houssais [bn], Vladimir Pospisil [ak], Baba Potukuchi [ch], Sidharth Kumar Prasad [dv], Roberto Preghenella [cu,l], Francesco Prino [cy], Claude Andre Pruneau [dv], Igor Pshenichnov [av], Giovanna Puddu [w], Valery Punin [cp], Marian Putis [al], Jorn Henning Putschke [dv], Emanuele Quercigh [ag], Henrik Qvigstad [u], Alexandre Rachevski [cz], Alphonse Rademakers [ag], Tomi Samuli Raiha [ap], Jan Rak [ap], Andry Malala Rakotozafindrabe [n], Luciano Ramello [ad], Abdiel Ramirez Reyes [k], Rashmi Raniwala [ci], Sudhir Raniwala [ci], Sami Sakari Rasanen [ap], Bogdan Theodor Rascanu [bd], Deepika Rathee [ce], Kenneth Francis Read [do], Jean-Sebastien Real [bo], Krzysztof Redlich [bu,bv], Rosi Jan Reed [dx], Attiq Ur Rehman [r], Patrick Reichelt [bd], Martijn Reicher [aw], Rainer Arno Ernst Renfordt [bd], Anna Rita Reolon [bp], Andrey Reshetin [av], Felix Vincenz Rettig [am], Jean-Pierre Revol [ag], Klaus Johannes Reygers [cj], Lodovico Riccati [cy], Renato Angelo Ricci [bq], Tuva Richert [af], Matthias Rudolph Richter [u], Petra Riedler [ag], Werner Riegler [ag], Francesco Riggi [z,db], Mario Rodriguez Cahuantzi [b], Alis Rodriguez Manso [bz], Ketil Roed [r,u], David Rohr [am], Dieter Rohrich [r], Rosa Romita [cn,dc], Federico Ronchetti [bp], Philippe Rosnet [bn], Stefan Rossegger [ag], Andrea Rossi [ag,ab], Christelle Sophie Roy [bi], Pradip Kumar Roy [cr], Antonio Juan Rubio Montero [j], Rinaldo Rui [x],

Riccardo Russo [v], Evgeny Ryabinkin [cq], Andrzej Rybicki [dg], Sergey Sadovsky [au], Karel Safarik [ag],
Raghunath Sahoo [as], Pradip Kumar Sahu [az], Jogender Saini [ds], Hiroaki Sakaguchi [aq], Shingo Sakai [br],
Dosatsu Sakata [dq], Carlos Albert Salgado [p], Jai Salzwedel [s], Sanjeev Singh Sambyal [ch],
Vladimir Samsonov [cc], Xitzel Sanchez Castro [bi], Ladislav Sandor [ay], Andres Sandoval [bh], Masato Sano [dq],
Gianluca Santagati [z], Romualdo Santoro [ag,l], Juho Jaako Sarkamo [ap], Eugenio Scapparone [cu],
Fernando Scarlassara [ab], Rolf Paul Scharenberg [cl], Claudiu Cornel Schiaua [bw], Rainer Martin Schicker [cj],
Christian Joachim Schmidt [cn], Hans Rudolf Schmidt [dr], Simone Schuchmann [bd], Jurgen Schukraft [ag],
Tim Schuster [dx], Yves Roland Schutz [ag,dd], Kilian Eberhard Schwarz [cn], Kai Oliver Schweda [cn],
Gilda Scioli [aa], Enrico Scomparin [cy], Patrick Aaron Scott [cs], Rebecca Scott [do], Gianfranco Segato [ab],
Ilya Selyuzhenkov [cn], Serhiy Senyukov [bi], Jeewon Seo [cm], Sergio Serci [w], Eulogio Serradilla [j,bh],
Adrian Sevcenco [bb], Alexandre Shabetai [dd], Galina Shabratova [bj], Ruben Shahoyan [ag], Natasha Sharma [ce,do],
Satish Sharma [ch], Rohini Sharma [ch], Kenta Shigaki [aq], Katherin Shtejer [i], Yury Sibiriak [cq], Eva Sicking [bf],
Sabyasachi Siddhanta [cx], Teodor Siemiarczuk [bu], David Olle Rickard Silvermyr [cb], Catherine Silvestre [bo],
Goran Simatovic [bg,co], Giuseppe Simonetti [ag], Rama Narayana Singaraju [ds], Ranbir Singh [ch],
Subhash Singha [ds,bx], Vikas Singhal [ds], Bikash Sinha [ds], Tinku Sinha [cr], Branislav Sitar [aj], Mario Sitta [ad],
Bernhard Skaali [u], Kyrre Skjerdal [r], Radek Smakal [ak], Nikolai Smirnov [dx], Raimond Snellings [aw],
Carsten Sogaard [by,af], Ron Ariel Soltz [bs], Hyungsuk Son [t], Jihye Song [cm], Myunggeun Song [dz], Csaba Soos [ag],
Francesca Soramel [ab], Iwona Sputowska [dg], Martha Spyropoulou-Stassinaki [cf], Brijesh Kumar Srivastava [cl],
Johanna Stachel [cj], Ionel Stan [bb], Grzegorz Stefanek [bu], Matthew Steinpreis [s], Evert Anders Stenlund [af],
Gideon Francois Steyn [cg], Johannes Hendrik Stiller [cj], Diego Stocco [dd], Mikhail Stolpovskiy [au],
Peter Strmen [aj], Alexandre Alarcon do Passo Suaide [dj], Martin Alfonso Subieta Vasquez [v], Toru Sugitate [aq],
Christophe Pierre Suire [at], Rishat Sultanov [ax], Michal Sumbera [ca], Tatjana Susa [co], Timothy Symons [br],
Alejandro Szanto de Toledo [dj], Imrich Szarka [aj], Adam Szczepankiewicz [dg,ag], Artur Krzysztof Szostak [r],
Maciej Szymanski [du], Jun Takahashi [dk], Daniel Jesus Tapia Takaki [at], Attilio Tarantola Peloni [bd],
Alfonso Tarazona Martinez [ag], Arturo Tauro [ag], Guillermo Tejeda Munoz [b], Adriana Telesca [ag],
Cristina Terrevoli [ae], Jochen Mathias Thader [cn], Deepa Thomas [aw], Raphael Noel Tieulent [dl],
Anthony Timmins [dm], David Tlusty [ak], Alberica Toia [am,ab,cv], Hisayuki Torii [dp], Luca Toscano [cy],
Victor Trubnikov [c], David Christopher Truesdale [s], Wladyslaw Henryk Trzaska [ap], Tomoya Tsuji [dp],
Alexandr Tumkin [cp], Rosario Turrisi [cv], Trine Spedstad Tveter [u], Jason Glyndwr Ulery [bd], Kjetil Ullaland [r],
Jochen Ulrich [bk,bc], Antonio Uras [dl], Jozef Urban [al], Guido Marie Urciuoli [cw], Gianluca Usai [w],
Michal Vajzer [ak,ca], Martin Vala [bj,ay], Lizardo Valencia Palomo [at], Sara Vallero [cj], Pierre Vande Vyvre [ag],
Marco van Leeuwen [aw], Luigi Vannucci [bq], Aurora Diozcora Vargas [b], Raghava Varma [ar], Maria Vasileiou [cf],
Andrey Vasiliev [cq], Vladimir Vechernin [dt], Misha Veldhoen [aw], Massimo Venaruzzo [x], Ermanno Vercellin [v],
Sergio Vergara [b], Renaud Vernet [h], Marta Verweij [aw], Linda Vickovic [df], Giuseppe Viesti [ab],
Jussi Viinikainen [ap], Zabulon Vilakazi [cg], Orlando Villalobos Baillie [cs], Yury Vinogradov [cp],
Alexander Vinogradov [cq], Leonid Vinogradov [dt], Tiziano Virgili [ac], Yogendra Viyogi [ds],
Alexander Vodopianov [bj], Sergey Voloshin [dv], Kirill Voloshin [ax], Giacomo Volpe [ag],
Barthelemy von Haller [ag], Ivan Vorobyev [dt], Danilo Vranic [cn], Janka Vrlakova [al], Bogdan Vulpescu [bn],
Alexey Vyushin [cp], Boris Wagner [r], Vladimir Wagner [ak], Renzhuo Wan [g], Yaping Wang [g], Yifei Wang [cj],
Mengliang Wang [g], Dong Wang [g], Kengo Watanabe [dq], Michael Weber [dm], Johannes Wessels [ag,bf],
Uwe Westerhoff [bf], Jens Wiechula [dr], Jon Wikne [u], Martin Rudolf Wilde [bf], Grzegorz Andrzej Wilk [bu],
Alexander Wilk [bf], Crispin Williams [cu], Bernd Stefan Windelband [cj], Leonidas Xaplanteris Karampatsos [dh],
Chris G. Yaldo [dv], Yorito Yamaguchi [dp], Hongyan Yang [n,aw], Shiming Yang [r], Stanislav Yasnopolsky [cq],
JunGyu Yi [cm], Zhongbao Yin [g], In-Kwon Yoo [cm], Jongik Yoon [dz], Weilin Yu [bd], Xianbao Yuan [g],
Igor Yushmanov [cq], Valentina Zaccolo [by], Cenek Zach [ak], Chiara Zampolli [cu], Sergey Zaporozhets [bj],
Andrey Zarochentsev [dt], Petr Zavada [ba], Nikolai Zaviyalov [cp], Hanna Paulina Zbroszczyk [du],
Pierre Zelnicek [bc], Sorin Ion Zgura [bb], Mikhail Zhalov [cc], Haitao Zhang [g], Xiaoming Zhang [br,bn,g],
Fengchu Zhou [g], You Zhou [aw], Daicui Zhou [g], Hongsheng Zhu [g], Jianhui Zhu [g], Jianlin Zhu [g],
Xiangrong Zhu [g], Antonino Zichichi [aa,l], Alice Zimmermann [cj], Gennady Zinovjev [c],
Yannick Denis Zoccarato [dl], Mykhaylo Zynovyev [c], Maksym Zyzak [bd]

---

[a] *A. I. Alikhanyan National Science Laboratory (Yerevan Physics Institute) Foundation, Yerevan, Armenia*
[b] *Benemérita Universidad Autónoma de Puebla, Puebla, Mexico*
[c] *Bogolyubov Institute for Theoretical Physics, Kiev, Ukraine*

[d] *Bose Institute, Department of Physics and Centre for Astroparticle Physics and Space Science (CAPSS), Kolkata, India*
[e] *Budker Institute for Nuclear Physics, Novosibirsk, Russia*
[f] *California Polytechnic State University, San Luis Obispo, CA, United States*
[g] *Central China Normal University, Wuhan, China*
[h] *Centre de Calcul de l'IN2P3, Villeurbanne, France*
[i] *Centro de Aplicaciones Tecnológicas y Desarrollo Nuclear (CEADEN), Havana, Cuba*
[j] *Centro de Investigaciones Energéticas Medioambientales y Tecnológicas (CIEMAT), Madrid, Spain*
[k] *Centro de Investigación y de Estudios Avanzados (CINVESTAV), Mexico City and Mérida, Mexico*
[l] *Centro Fermi – Museo Storico della Fisica e Centro Studi e Ricerche "Enrico Fermi", Rome, Italy*
[m] *Chicago State University, Chicago, IL, United States*
[n] *Commissariat à l'Energie Atomique, IRFU, Saclay, France*
[o] *COMSATS Institute of Information Technology (CIIT), Islamabad, Pakistan*
[p] *Departamento de Física de Partículas and IGFAE, Universidad de Santiago de Compostela, Santiago de Compostela, Spain*
[q] *Department of Physics Aligarh Muslim University, Aligarh, India*
[r] *Department of Physics and Technology, University of Bergen, Bergen, Norway*
[s] *Department of Physics, Ohio State University, Columbus, OH, United States*
[t] *Department of Physics, Sejong University, Seoul, South Korea*
[u] *Department of Physics, University of Oslo, Oslo, Norway*
[v] *Dipartimento di Fisica dell'Università and Sezione INFN, Turin, Italy*
[w] *Dipartimento di Fisica dell'Università and Sezione INFN, Cagliari, Italy*
[x] *Dipartimento di Fisica dell'Università and Sezione INFN, Trieste, Italy*
[y] *Dipartimento di Fisica dell'Università 'La Sapienza' and Sezione INFN, Rome, Italy*
[z] *Dipartimento di Fisica e Astronomia dell'Università and Sezione INFN, Catania, Italy*
[aa] *Dipartimento di Fisica e Astronomia dell'Università and Sezione INFN, Bologna, Italy*
[ab] *Dipartimento di Fisica e Astronomia dell'Università and Sezione INFN, Padova, Italy*
[ac] *Dipartimento di Fisica 'E.R. Caianiello' dell'Università and Gruppo Collegato INFN, Salerno, Italy*
[ad] *Dipartimento di Scienze e Innovazione Tecnologica dell'Università del Piemonte Orientale and Gruppo Collegato INFN, Alessandria, Italy*
[ae] *Dipartimento Interateneo di Fisica 'M. Merlin' and Sezione INFN, Bari, Italy*
[af] *Division of Experimental High Energy Physics, University of Lund, Lund, Sweden*
[ag] *European Organization for Nuclear Research (CERN), Geneva, Switzerland*
[ah] *Fachhochschule Köln, Köln, Germany*
[ai] *Faculty of Engineering, Bergen University College, Bergen, Norway*
[aj] *Faculty of Mathematics, Physics and Informatics, Comenius University, Bratislava, Slovakia*
[ak] *Faculty of Nuclear Sciences and Physical Engineering, Czech Technical University in Prague, Prague, Czech Republic*
[al] *Faculty of Science, P.J. Šafárik University, Košice, Slovakia*
[am] *Frankfurt Institute for Advanced Studies, Johann Wolfgang Goethe-Universität Frankfurt, Frankfurt, Germany*
[an] *Gangneung-Wonju National University, Gangneung, South Korea*
[ao] *Gauhati University, Department of Physics, Guwahati, India*
[ap] *Helsinki Institute of Physics (HIP) and University of Jyväskylä, Jyväskylä, Finland*
[aq] *Hiroshima University, Hiroshima, Japan*
[ar] *Indian Institute of Technology Bombay (IIT), Mumbai, India*
[as] *Indian Institute of Technology Indore (IITI), Indore, India*
[at] *Institut de Physique Nucléaire d'Orsay (IPNO), Université Paris-Sud, CNRS–IN2P3, Orsay, France*
[au] *Institute for High Energy Physics, Protvino, Russia*
[av] *Institute for Nuclear Research, Academy of Sciences, Moscow, Russia*
[aw] *Nikhef, National Institute for Subatomic Physics and Institute for Subatomic Physics of Utrecht University, Utrecht, Netherlands*
[ax] *Institute for Theoretical and Experimental Physics, Moscow, Russia*
[ay] *Institute of Experimental Physics, Slovak Academy of Sciences, Košice, Slovakia*
[az] *Institute of Physics, Bhubaneswar, India*
[ba] *Institute of Physics, Academy of Sciences of the Czech Republic, Prague, Czech Republic*
[bb] *Institute of Space Sciences (ISS), Bucharest, Romania*
[bc] *Institut für Informatik, Johann Wolfgang Goethe-Universität Frankfurt, Frankfurt, Germany*
[bd] *Institut für Kernphysik, Johann Wolfgang Goethe-Universität Frankfurt, Frankfurt, Germany*
[be] *Institut für Kernphysik, Technische Universität Darmstadt, Darmstadt, Germany*
[bf] *Institut für Kernphysik, Westfälische Wilhelms-Universität Münster, Münster, Germany*
[bg] *Instituto de Ciencias Nucleares, Universidad Nacional Autónoma de México, Mexico City, Mexico*
[bh] *Instituto de Física, Universidad Nacional Autónoma de México, Mexico City, Mexico*
[bi] *Institut Pluridisciplinaire Hubert Curien (IPHC), Université de Strasbourg, CNRS-IN2P3, Strasbourg, France*
[bj] *Joint Institute for Nuclear Research (JINR), Dubna, Russia*
[bk] *Kirchhoff-Institut für Physik, Ruprecht-Karls-Universität Heidelberg, Heidelberg, Germany*
[bl] *Korea Institute of Science and Technology Information, Daejeon, South Korea*
[bm] *KTO Karatay University, Konya, Turkey*
[bn] *Laboratoire de Physique Corpusculaire (LPC), Clermont Université, Université Blaise Pascal, CNRS–IN2P3, Clermont-Ferrand, France*
[bo] *Laboratoire de Physique Subatomique et de Cosmologie (LPSC), Université Joseph Fourier, CNRS-IN2P3, Institut Polytechnique de Grenoble, Grenoble, France*
[bp] *Laboratori Nazionali di Frascati, INFN, Frascati, Italy*
[bq] *Laboratori Nazionali di Legnaro, INFN, Legnaro, Italy*
[br] *Lawrence Berkeley National Laboratory, Berkeley, CA, United States*
[bs] *Lawrence Livermore National Laboratory, Livermore, CA, United States*
[bt] *Moscow Engineering Physics Institute, Moscow, Russia*
[bu] *National Centre for Nuclear Studies, Warsaw, Poland*
[bv] *Institute of Theoretical Physics, University of Wroclaw, Wroclaw, Poland*
[bw] *National Institute for Physics and Nuclear Engineering, Bucharest, Romania*
[bx] *National Institute of Science Education and Research, Bhubaneswar, India*
[by] *Niels Bohr Institute, University of Copenhagen, Copenhagen, Denmark*
[bz] *Nikhef, National Institute for Subatomic Physics, Amsterdam, Netherlands*
[ca] *Nuclear Physics Institute, Academy of Sciences of the Czech Republic, Řež u Prahy, Czech Republic*
[cb] *Oak Ridge National Laboratory, Oak Ridge, TN, United States*
[cc] *Petersburg Nuclear Physics Institute, Gatchina, Russia*
[cd] *Physics Department, Creighton University, Omaha, NE, United States*

ce *Physics Department, Panjab University, Chandigarh, India*
cf *Physics Department, University of Athens, Athens, Greece*
cg *Physics Department, University of Cape Town and iThemba LABS, National Research Foundation, Somerset West, South Africa*
ch *Physics Department, University of Jammu, Jammu, India*
ci *Physics Department, University of Rajasthan, Jaipur, India*
cj *Physikalisches Institut, Ruprecht-Karls-Universität Heidelberg, Heidelberg, Germany*
ck *Politecnico di Torino, Turin, Italy*
cl *Purdue University, West Lafayette, IN, United States*
cm *Pusan National University, Pusan, South Korea*
cn *Research Division and ExtreMe Matter Institute EMMI, GSI Helmholtzzentrum für Schwerionenforschung, Darmstadt, Germany*
co *Rudjer Bošković Institute, Zagreb, Croatia*
cp *Russian Federal Nuclear Center (VNIIEF), Sarov, Russia*
cq *Russian Research Centre Kurchatov Institute, Moscow, Russia*
cr *Saha Institute of Nuclear Physics, Kolkata, India*
cs *School of Physics and Astronomy, University of Birmingham, Birmingham, United Kingdom*
ct *Sección Física, Departamento de Ciencias, Pontificia Universidad Católica del Perú, Lima, Peru*
cu *Sezione INFN, Bologna, Italy*
cv *Sezione INFN, Padova, Italy*
cw *Sezione INFN, Rome, Italy*
cx *Sezione INFN, Cagliari, Italy*
cy *Sezione INFN, Turin, Italy*
cz *Sezione INFN, Trieste, Italy*
da *Sezione INFN, Bari, Italy*
db *Sezione INFN, Catania, Italy*
dc *Nuclear Physics Group, STFC Daresbury Laboratory, Daresbury, United Kingdom*
dd *SUBATECH, Ecole des Mines de Nantes, Université de Nantes, CNRS-IN2P3, Nantes, France*
de *Suranaree University of Technology, Nakhon Ratchasima, Thailand*
df *Technical University of Split FESB, Split, Croatia*
dg *The Henryk Niewodniczanski Institute of Nuclear Physics, Polish Academy of Sciences, Cracow, Poland*
dh *The University of Texas at Austin, Physics Department, Austin, TX, United States*
di *Universidad Autónoma de Sinaloa, Culiacán, Mexico*
dj *Universidade de São Paulo (USP), São Paulo, Brazil*
dk *Universidade Estadual de Campinas (UNICAMP), Campinas, Brazil*
dl *Université de Lyon, Université Lyon 1, CNRS/IN2P3, IPN-Lyon, Villeurbanne, France*
dm *University of Houston, Houston, TX, United States*
dn *University of Technology and Austrian Academy of Sciences, Vienna, Austria*
do *University of Tennessee, Knoxville, Tennessee, United States*
dp *University of Tokyo, Tokyo, Japan*
dq *University of Tsukuba, Tsukuba, Japan*
dr *Eberhard Karls Universität Tübingen, Tübingen, Germany*
ds *Variable Energy Cyclotron Centre, Kolkata, India*
dt *V. Fock Institute for Physics, St. Petersburg State University, St. Petersburg, Russia*
du *Warsaw University of Technology, Warsaw, Poland*
dv *Wayne State University, Detroit, MI, United States*
dw *Wigner Research Centre for Physics, Hungarian Academy of Sciences, Budapest, Hungary*
dx *Yale University, New Haven, CT, United States*
dy *Yildiz Technical University, Istanbul, Turkey*
dz *Yonsei University, Seoul, South Korea*
ea *Zentrum für Technologietransfer und Telekommunikation (ZTT), Fachhochschule Worms, Worms, Germany*

* Corresponding author.
 E-mail address: jgrosseo@cern.ch (J.F. Grosse-Oetringhaus).
 i M.V. Lomonosov Moscow State University, D.V. Skobeltsyn Institute of Nuclear Physics, Moscow, Russia.
 ii University of Belgrade, Faculty of Physics and "Vinča" Institute of Nuclear Sciences, Belgrade, Serbia.